Eur. Phys. J. A **19**, 423–438 (2004)
DOI 10.1140/epja/i2003-10127-x

THE EUROPEAN PHYSICAL JOURNAL A

Deep electroproduction of photons and mesons on the deuteron

F. Cano[1] and B. Pire[2,a]

[1] DAPNIA/SPhN, CEA-Saclay, F-91191 Gif-sur-Yvette Cedex, France
[2] CPhT, École Polytechnique, (UMR C7644 of CNRS), F-91128 Palaiseau Cedex, France

Received: 21 July 2003 / Revised version: 9 September 2003 /
Published online: 5 February 2004 –
Communicated by V. Vento

Abstract. We study deeply virtual Compton scattering and deep exclusive meson electroproduction on a deuteron target. We model the generalized quark distributions in the deuteron by using the impulse approximation for the lowest Fock-space state on the light cone. We study the properties of the resulting GPDs, and verify that sum rules violations are quite small in the impulse approximation. Numerical predictions are given for the unpolarized cross-sections and polarization asymmetries for the kinematical regimes relevant for JLab experiments and for HERMES at HERA. We conclude that the signal of coherent scattering on the deuteron is comparable to the one on the proton at least for low momentum transfer, providing support to the feasibility of the experiments. The short-distance structure of the deuteron may thus be scrutinized in the near future.

PACS. 24.85.+p Quarks, gluons, and QCD in nuclei and nuclear processes – 12.38.Bx Perturbative calculations – 25.30.-c Lepton-induced reactions

1 Introduction

The study of hard exclusive processes, such as deeply Virtual Compton Scattering (DVCS),

$$eA \to e'\gamma A' \tag{1}$$

and deep exclusive meson electroproduction (DEMP)

$$eA \to e'MA', \tag{2}$$

where A is a hadron (usually a nucleon, here a deuteron), and M a meson (usually a ρ or a π) or a pair of mesons (of relatively small invariant mass) in the kinematical domain of a large momentum transfer Q^2 between the leptons but a small momentum transfer (t) between the hadrons, has been recently demonstrated to open the possibility of obtaining a quite complete picture of the hadronic structure. The information which can be accessed through these experiments is encoded by the generalized parton distributions, GPDs [1,2] (for recent reviews see [3]), which give in particular information on the transverse location of quarks in the hadrons [4]. Recent measurements of the azimuthal dependence of the beam spin asymmetry in DVCS [5,6] have provided experimental evidence to support the validity of the formalism of GPDs and the underlying QCD factorization of short-distance and long-distance dominated subprocesses.

The theoretical arguments used in deriving factorization theorems in QCD for the nucleon [7] target case can be applied to the deuteron case as well, and therefore one can develop the formalism of GPDs for the deuteron [8]. From the theoretical viewpoint, it is the simplest and best known nuclear system and represents the most appropriate starting point to investigate hard exclusive processes off nuclei [9]. On the other hand, these processes could offer a new source of information about the partonic degrees of freedom in nuclei, complementary to the existing one from deep inelastic scattering. Experimentally, deuteron targets are quite common and as a matter of fact, DVCS experiments are being planned or carried out at facilities like CEBAF at JLab and HERMES at HERA, where some data have already been released [10]. One should, of course, distinguish the case where the deuteron serves merely as a source of slightly bound protons and neutrons from the case where the deuteron acts as a single hadron. In the former case, the scattering is incoherent and the deuteron will break up during the reaction. In the latter case, to which we devote our study, the deuteron stays intact after the scattering. The fact that this occurs in a non-negligible fraction of events is not evident to everybody, since it is usual, but uncorrect, to mix the concepts of hard and destructive reactions. Indeed, as estimates given below will show, the very nature of deep electroproduction in the forward region is that the target is not violently shattered by the hard probe. The fragile nature of

[a] e-mail: pire@cpht.polytechnique.fr

the deuteron thus does not prevent it from staying intact. This picture should, of course, be experimentally tested through the comparison of rates for coherent and incoherent electroproduction. The need for a deuteron recoil detector is primordial in this respect.

The paper is organized as follows: in sect. 2 we remind the reader of the formalism of generalized parton distributions for spin-1 targets in general and the deuteron in particular. In sect. 3, we explain in detail the construction of the impulse approximation to evaluate the helicity amplitudes and in sect. 4 we derive the deuteron GPDs from the helicity amplitudes and study the properties and implications with a numerical model. In sect. 5 we give the useful formulae for calculating the DVCS cross-section. In sect. 6 we show our numerical estimates for the usual observables in the DVCS case and comment on the feasibility of experiments. In sect. 7 we examine the electroproduction of mesons. Througout the paper we will limit ourselves to the quark sector of the GPDs, which is a good approximation provided the Bjorken variable $x_{\rm Bj}$ is not too small. This variable is defined as usual as $x_{\rm Bj} = \frac{Q^2}{2P\cdot q}$, *i.e.*, it is given in lab frame by $x_{\rm Bj} = \frac{Q^2}{2M\nu}$, where M is the deuteron mass and ν the virtual photon energy. Gluon effects will be needed for understanding higher-energies experiments. Previous short reports on our results have been presented at recent conferences [11].

2 GPDs in the deuteron: definitions and basic properties

A parameterization of the non-perturbative matrix elements which determine the amplitudes in DVCS and DEMP on a spin-one target was given in terms of nine GPDs for the quark sector [8]:

$$V_{\lambda'\lambda} = \int \frac{\mathrm{d}\kappa}{2\pi}\, e^{ix\kappa 2\bar{P}\cdot n} \langle P',\lambda'|\, \bar{\psi}(-\kappa n)\, \gamma\cdot n\, \psi(\kappa n)\, |P,\lambda\rangle$$
$$= \sum_{i=1,5} \epsilon'^{*\beta} V^{(i)}_{\beta\alpha}\, \epsilon^{\alpha}\, H_i(x,\xi,t), \tag{3}$$

$$A_{\lambda'\lambda} = \int \frac{\mathrm{d}\kappa}{2\pi}\, e^{ix\kappa 2\bar{P}\cdot n} \langle P',\lambda'|\, \bar{\psi}(-\kappa n)\, \gamma\cdot n\gamma_5\, \psi(\kappa n)\, |P,\lambda\rangle$$
$$= \sum_{i=1,4} \epsilon'^{*\beta} A^{(i)}_{\beta\alpha}\, \epsilon^{\alpha}\, \tilde{H}_i(x,\xi,t), \tag{4}$$

where $|P,\lambda\rangle$ represents a deuteron state of momentum P and polarization λ, $\bar{P} = (P+P')/2$, and n^μ is a light-like vector with $n^+ = 0$, $\mathbf{n}_\perp = 0$. Due to the spin-one character of the target, there are more GPDs than in the nucleon case, but at the same time the set of polarization observables which in principle could be measured is also richer. Not much is known about these non-perturbative objects which encode the way quarks are confined in deuterons, except a limited set of sum rules and some limiting case values. Sum rules [8] relate these GPDs to the usual deuteron form factors:

$$\int_{-1}^{1} \mathrm{d}x H_i(x,\xi,t) = G_i(t) \qquad (i=1,2,3),$$
$$\int_{-1}^{1} \mathrm{d}x \tilde{H}_i(x,\xi,t) = \tilde{G}_i(t) \qquad (i=1,2), \tag{5}$$

or lead to a null average:

$$\int_{-1}^{1} \mathrm{d}x H_4(x,\xi,t) = \int_{-1}^{1} \mathrm{d}x \tilde{H}_3(x,\xi,t) \;=\; 0,$$
$$\int_{-1}^{1} \mathrm{d}x H_5(x,\xi,t) = \int_{-1}^{1} \mathrm{d}x \tilde{H}_4(x,\xi,t) \;=\; 0. \tag{6}$$

Taking the forward limit of the matrix elements defining GPDs leads to the relations [8] between GPDs and parton densities in the deuteron (with obvious notations) as

$$H_1(x,0,0) = \frac{q^1(x)+q^{-1}(x)+q^0(x)}{3},$$
$$H_5(x,0,0) = q^0(x) - \frac{q^1(x)+q^{-1}(x)}{2},$$
$$\tilde{H}_1(x,0,0) = q^1_\uparrow(x) - q^{-1}_\uparrow(x) \tag{7}$$

for $x>0$. The corresponding relations for $x<0$ involve the antiquark distributions at $-x$, with an overall minus sign in the expressions for H_1 and H_5.

In all this paper we will restrict to the quark contribution. Gluon contributions are expected to be small at medium energies but should be included in a more complete description of the process. Therefore, we will limit ourselves to values of $x_{\rm Bj}$ not smaller than 0.1.

3 Helicity amplitudes in the impulse approximation

The impulse approximation (fig. 1) is the zeroth order to explain the photon-nucleus interaction, but it is the first model one has to analyze since the bulk of the physics is already contained in it.

In the previous section we mentioned that the relevant quantities are the deuteron GPDs. For the sake of simplicity, we will model the matrix elements $V_{\lambda'\lambda}$ (3) and $A_{\lambda'\lambda}$ (4) and recover the GPDs just by using the relations given in the appendix. Furthermore, since we are going to limit ourselves to the quark content of the deuteron and this is an isoscalar target, we will set

$$V^u_{\lambda'\lambda} = V^d_{\lambda'\lambda} \equiv V^q_{\lambda'\lambda} \tag{8}$$

and a similar relation holds for $A_{\lambda'\lambda}$.

Let us denote by P^μ (P'^μ) the momentum of the incoming (outgoing) deuteron and λ (λ') its polarization state, that sometimes we will denote by $0,+$ or $-$. To perform this analysis, we will choose a symmetric frame where the average momentum $\bar{P}^\mu = (P^\mu + P'^\mu)/2$ has no transverse components. We will also need a light-like

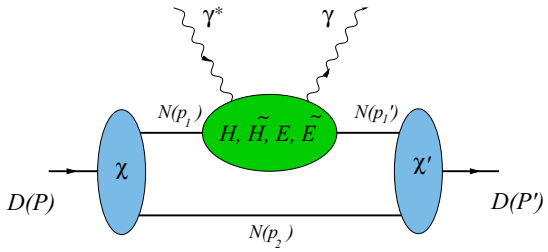

Fig. 1. Estimating the helicity amplitudes for the $\gamma^* D \to \gamma D$ in the impulse approximation. The final result is a convolution model between the deuteron wave function and the GPDs for the nucleon (upper blob).

vector n^μ to define, together with $\bar{P}^\mu$, the light cone and satisfying $\bar{P}\cdot n = 1$. To be more concrete, it is convenient to choose a frame where $\bar{P}^\mu$ moves fast to the right.

The momentum transfer $\Delta^\mu = P'^\mu - P^\mu$ has a longitudinal and a transverse component. The skewness controls the fraction of momentum transferred in the "+" direction:

$$\xi = -\frac{\Delta\cdot n}{(P+P')\cdot n} = -\frac{\Delta^+}{2\bar{P}^+}. \tag{9}$$

With these considerations, the four-vectors corresponding to each deuteron are[1]

$$P^\mu = \left((1+\xi)\bar{P}^+, \frac{M^2+\boldsymbol{\Delta}_\perp^2/2}{2\bar{P}^+(1+\xi)}, -\frac{\boldsymbol{\Delta}_\perp}{2}\right), \tag{10}$$

$$P'^\mu = \left((1-\xi)\bar{P}^+, \frac{M^2+\boldsymbol{\Delta}_\perp^2/2}{2\bar{P}^+(1-\xi)}, \frac{\boldsymbol{\Delta}_\perp}{2}\right). \tag{11}$$

The invariant momentum transfer is written as

$$t = \Delta^2 = -\frac{4\xi^2 M^2 + \boldsymbol{\Delta}_\perp^2}{1-\xi^2}. \tag{12}$$

The positivity of $\boldsymbol{\Delta}_\perp^2$ implies that there is a minimal momentum transfer t_0 for a fixed ξ:

$$t_0 = -\frac{4\xi^2 M^2}{1-\xi^2}, \tag{13}$$

and at the same time, for a given t, there is un upper bound on the allowed values for ξ:

$$\xi^2 \le \frac{-t}{4M^2 - t}. \tag{14}$$

The GPDs depend in addition on one more variable x which is defined as the fraction of average momentum carried by the partons in the "+" direction:

$$x = \frac{\bar{k}\cdot n}{\bar{P}\cdot n} \tag{15}$$

with $\bar{k}^\mu = (k^\mu + k'^\mu)/2$. Therefore, the longitudinal momentum of the initial parton is $(x+\xi)\bar{P}^+$, whereas the final one has $(x-\xi)\bar{P}^+$, delivering a longitudinal transfer $\Delta^+ = -2\xi\bar{P}^+$ to the deuteron.

Now let us turn our attention to the kinematics at the nucleon level and let us define the fraction of longitudinal momentum carried by each nucleon in the deuteron as

$$\alpha_i = \frac{p_i^+}{P^+}, \qquad \alpha_i' = \frac{p_i'^+}{P'^+}. \tag{16}$$

Therefore, we have that the relevant kinematical quantities for the nucleons that make up the initial deuteron are ($\alpha \equiv \alpha_1$)

$$\begin{aligned} p_1^+ &= \alpha(1+\xi)\bar{P}^+, \\ p_2^+ &= (1-\alpha)(1+\xi)\bar{P}^+, \\ \mathbf{p}_{1\perp} + \mathbf{p}_{2\perp} &= -\frac{\boldsymbol{\Delta}_\perp}{2}. \end{aligned} \tag{17}$$

and for the final deuteron we have ($\alpha' \equiv \alpha_1'$)

$$\begin{aligned} p_1'^+ &= \alpha'(1-\xi)\bar{P}^+, \\ p_2'^+ &= (1-\alpha')(1-\xi)\bar{P}^+, \\ \mathbf{p}'_{1\perp} + \mathbf{p}'_{2\perp} &= \frac{\boldsymbol{\Delta}_\perp}{2}. \end{aligned} \tag{18}$$

We can now use the decomposition of the deuteron states in terms of nucleon states and the wave function defined in appendix A.1, eq. (A.2), to get

$$\begin{aligned} V^q_{\lambda'\lambda} = \frac{2}{(16\pi^3)}\int \mathrm{d}\alpha\,\mathrm{d}\alpha'\,\mathrm{d}\mathbf{p}_{1\perp}\mathrm{d}\mathbf{p}'_{1\perp}\sqrt{\frac{1+\xi}{1-\xi}}\frac{1}{\sqrt{\alpha\alpha'}} \\ \cdot \delta^2(\mathbf{p}'_{1\perp} - \mathbf{p}_{1\perp} - \boldsymbol{\Delta}_\perp)\delta\left(\alpha' - \frac{\alpha(1+\xi)-2\xi}{1-\xi}\right) \\ \cdot \Theta(\alpha(1+\xi) - |x| - \xi)\ \Theta(\alpha(1+\xi) - 2\xi) \\ \cdot \sum_{\lambda_1',\lambda_1,\lambda_2} \chi^*_{\lambda'}(\alpha', \mathbf{k}'_\perp, \lambda_1', \lambda_2)\chi_\lambda(\alpha, \mathbf{k}_\perp, \lambda_1, \lambda_2) \\ \cdot \frac{1}{2}\int \frac{\mathrm{d}\kappa}{2\pi} e^{i\kappa x}\left\langle p_1', \lambda_1'|\bar{\psi}_q\left(-\frac{\kappa}{2}n\right)\gamma\cdot n\psi_q\left(\frac{\kappa}{2}n\right)|p_1,\lambda_1\right\rangle. \end{aligned} \tag{19}$$

In the equation above, the variables of the spectator nucleon have been eliminated just by using the normalization properties of the one-particle states. The arguments of the deuteron wave function (see appendix A.1 for details), $\mathbf{k}'_\perp$ and $\mathbf{k}_\perp$, are the transverse momenta of the active nucleon in a frame where $\mathbf{P}'_\perp = 0$ and $\mathbf{P}_\perp = 0$, respectively. Their relationship with the transverse momenta in the symmetric frame is

$$\mathbf{k}_\perp \equiv \mathbf{k}_{1_\perp} = \mathbf{p}_{1_\perp} + \alpha\frac{\boldsymbol{\Delta}_\perp}{2}, \tag{20}$$

$$\mathbf{k}'_\perp \equiv \mathbf{k}'_{1_\perp} = \mathbf{p}'_{1_\perp} - \alpha'\frac{\boldsymbol{\Delta}_\perp}{2}. \tag{21}$$

The Heaviside functions in eq. (19) ensure the positivity of the "plus" momentum carried by the nucleons and put a lower bound on the integration over α. The first one

[1] We use the following notation for the four-vectors: $(v^+, v^-, \mathbf{v}_\perp)$, with $v^\pm = \frac{1}{\sqrt{2}}(v^0 \pm v^3)$.

stands for processes where $|x| > \xi$, whereas the second one acts when we are on the ERBL region where $|x| < \xi$.

Therefore, we end up with matrix elements of a non-local quark operator between one-nucleon states, which is parameterized in terms of nucleon GPDs. To take advantage of usual parameterizations found in the literature, it is convenient to keep on working on a symmetric frame. However, since nucleons carry some transverse momentum within the deuteron, the symmetric frame for the deuteron is not the symmetric frame for the active nucleon.

By performing a transverse boost, it is possible to evaluate the matrix element in (19) in a symmetric frame, which has the property

$$\tilde{\mathbf{p}}'_{1_\perp} + \tilde{\mathbf{p}}_{1_\perp} = 0, \tag{22}$$

where we have marked with a $\tilde{}$ the quantities in this boosted frame. Since it is a transverse boost, it does not change the "+" components of the vectors. The light-like vector n^μ is not changed either, since it is a light-like vector with no transverse components, *i.e.* $\tilde{n}^\mu = n^\mu$.

In that frame, the parameterization of the nucleon GPDs is made with variables that refer to the initial and final nucleon, *i.e.*, we define

$$x_N = \frac{\bar{\tilde{k}} \cdot \tilde{n}}{\bar{\tilde{p}}_1 \cdot \tilde{n}} = \frac{x}{\alpha(1+\xi) - \xi}, \tag{23}$$

$$\xi_N = -\frac{\tilde{\Delta} \cdot \tilde{n}}{2\bar{\tilde{p}}_1 \cdot \tilde{n}} = \frac{\xi}{\alpha(1+\xi) - \xi}. \tag{24}$$

Due to the lower bound on the values of α, we have $\xi_N \geq \xi$. Moreover, it can be checked that $\frac{x}{\xi} = \frac{x_N}{\xi_N}$, which is consistent with the fact that we are probing $q\bar{q}$ distribution amplitudes in the deuteron only through the nucleon. In other words, when we enter the ERBL region in the deuteron (*i.e.* when $|x| = \xi$), we do so at the nucleon level (*i.e.* when $|x_N| = \xi_N$).

The transverse momentum of the nucleon that interacts with the photon is, after the boost,

$$\tilde{\mathbf{p}}_{1_\perp} = -\frac{\tilde{\mathbf{\Delta}}_\perp}{2}, \tag{25}$$

$$\tilde{\mathbf{p}}'_{1_\perp} = \frac{\tilde{\mathbf{\Delta}}_\perp}{2}, \tag{26}$$

$$\tilde{\mathbf{\Delta}}_\perp = (1+\xi_N)\mathbf{\Delta}_\perp + 2\xi_N \mathbf{p}_{1_\perp}. \tag{27}$$

Now we can use the parameterization of the nucleon matrix element given in the appendix, and after some algebra and changes in the integration variables we reach the final result for $V_{\lambda'\lambda}$:

$$\begin{aligned} V^q_{\lambda'\lambda} = {} & \frac{2}{(16\pi^3)} \int_{\alpha_{\min}} \mathrm{d}\alpha \mathrm{d}\alpha' \mathrm{d}\mathbf{k}_\perp \mathrm{d}\mathbf{k}'_\perp \sqrt{\frac{1+\xi}{1-\xi}} \frac{1}{\sqrt{\alpha\alpha'}} \\ & \cdot \delta^2 \left(\mathbf{k}'_\perp - \mathbf{k}_\perp - \left(\frac{1-\alpha}{1-\xi} \right) \mathbf{\Delta}_\perp \right) \delta \left(\alpha' - \frac{\alpha(1+\xi) - 2\xi}{1-\xi} \right) \\ & \cdot \sum_{\lambda'_1, \lambda_1, \lambda_2} \chi^*_{\lambda'}(\alpha', \mathbf{k}'_\perp, \lambda'_1, \lambda_2) \chi_\lambda(\alpha, \mathbf{k}_\perp, \lambda_1, \lambda_2) \\ & \cdot \Bigg[\left(\sqrt{1-\xi_N^2} H^{\mathrm{IS}}(x_N, \xi_N, t) \right. \\ & \left. - \frac{\xi_N^2}{\sqrt{1-\xi_N^2}} E^{\mathrm{IS}}(x_N, \xi_N, t) \right) \delta_{\lambda'_1 \lambda_1} \\ & + \frac{\sqrt{t_0 - t}}{2m} \eta_{\lambda_1} E^{\mathrm{IS}}(x_N, \xi_N, t) \delta_{\lambda'_1, -\lambda_1} \Bigg] \end{aligned} \tag{28}$$

and a similar expression for $A^q_{\lambda'\lambda}$:

$$\begin{aligned} A^q_{\lambda'\lambda} = {} & \frac{2}{(16\pi^3)} \int_{\alpha_{\min}} \mathrm{d}\alpha \mathrm{d}\alpha' \mathrm{d}\mathbf{k}_\perp \mathrm{d}\mathbf{k}'_\perp \sqrt{\frac{1+\xi}{1-\xi}} \frac{1}{\sqrt{\alpha\alpha'}} \\ & \cdot \delta^2 \left(\mathbf{k}'_\perp - \mathbf{k}_\perp - \left(\frac{1-\alpha}{1-\xi} \right) \mathbf{\Delta}_\perp \right) \delta \left(\alpha' - \frac{\alpha(1+\xi) - 2\xi}{1-\xi} \right) \\ & \cdot \sum_{\lambda'_1, \lambda_1, \lambda_2} \chi^*_{\lambda'}(\alpha', \mathbf{k}'_\perp, \lambda'_1, \lambda_2) \chi_\lambda(\alpha, \mathbf{k}_\perp, \lambda_1, \lambda_2) \\ & \cdot \Bigg[2\lambda_1 \left(\sqrt{1-\xi_N^2} \tilde{H}^{\mathrm{IS}}(x_N, \xi_N, t) \right. \\ & \left. - \frac{\xi_N^2}{\sqrt{1-\xi_N^2}} \tilde{E}^{\mathrm{IS}}(x_N, \xi_N, t) \right) \delta_{\lambda'_1 \lambda_1} \\ & + 2\lambda_1 \xi_N \frac{\sqrt{t_0 - t}}{2m} \eta_{\lambda_1} \tilde{E}^{\mathrm{IS}}(x_N, \xi_N, t) \delta_{\lambda'_1, -\lambda_1} \Bigg]. \end{aligned} \tag{29}$$

The factor 2 in front of the formulae above stands for the number of nucleons, so that the isoscalar nucleon GPDs (H^{IS}, E^{IS}, ...) is the isoscalar combination within one single nucleon:

$$H^{\mathrm{IS}}(x_N, \xi_N, t) = \frac{1}{2} \left[H^u(x_N, \xi_N, t) + H^d(x_N, \xi_N, t) \right]. \tag{30}$$

The phase that goes with the nucleon helicity flip GPDs is given by

$$\eta_\lambda = \frac{2\lambda \tilde{\Delta}_x - i\tilde{\Delta}_y}{|\tilde{\Delta}_\perp|}. \tag{31}$$

For the sake of clarity, we have omitted the Heaviside function in the integrals above but recall that there is a lower bound on the value of α, which is

$$\alpha_{\min} = \max \left\{ \frac{2\xi}{1+\xi}, \frac{|x| + \xi}{1+\xi} \right\}. \tag{32}$$

4 Deuterons GPDs

Once we have obtained the helicity amplitudes, it is straightforward to get from them the deuteron GPDs (fig. 2), just from the definitions given in eqs. (3), (4). To do so in a simple way, one can use the light-cone polarization vectors given in [8]. The analytical expressions are summarized in the appendix.

At this point one may argue that definitions of deuteron GPDs were not actually necessary to reach the results of the preceding section and that one can derive

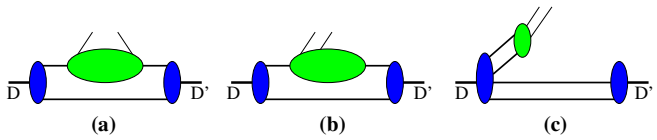

Fig. 2. Deuteron generalized parton distributions in the impulse (a and b) and beyond (c) the impulse approximation.

the cross-sections and observables, directly from eqs. (28) and (29). But it should be emphasized that the genuine objects that parameterize the hadronic structure are the GPDs, the rest being just kinematics. The GPDs have well-defined properties in some limits and their analysis could help us in testing the soundness of a model, as a complementary check to the comparison with experimental data.

4.1 Deuteron wave function

We need a specific model for the spatial deuteron wave function. As can be seen in the appendix, in the lower Fock-space approximation one can link the light cone wave function to the usual instant-form wave function through an identification of variables. We have chosen a parameterization of the spatial wave function given by the Paris potential [12] which has an S-wave supplemented with a D-wave component with a probability of 5.8%. We do not expect a strong dependence on the chosen parameterization for the deuteron wave function. Most of them are identical in the low-momentum region since they are strongly constrained by the well-known form factors. Differences between parameterizations are significant only in the large-momentum region. Since we are going to limit ourselves to the low-momentum-transfer region, we will not be especially sensitive to the tail of the wave function.

Nonetheless, before going through the details of the results, let us discuss some features of the deuteron GPDs that may be expected from quite general grounds. The skewness parameter ξ determines the momentum transfer in the longitudinal direction:

$$\Delta^+ \equiv (P'^+ - P^+) = -2\xi \bar{P}^+ \quad , \tag{33}$$

and in the generalized Bjorken limit this is entirely fixed by the kinematics of the virtual photon ($\xi \approx x_{\rm Bj}/2$). In the impulse approximation, this momentum transfer has to be provided by the active nucleon, and after that, the final state of this active nucleon still has to fit into the final deuteron. Since the deuteron is a loosely bound system, one cannot have a very asymmetrical sharing of longitudinal momentum between the nucleons and one may thus guess that the formation of the coherent final state will be strongly suppressed in the impulse approximation for large skewness.

To be more quantitative, let us define the longitudinal momentum distribution of the nucleon in the deuteron as

$$n_\lambda(\alpha) = \sum_{\lambda_1,\lambda_2} \int \frac{{\rm d}\mathbf{k}_\perp {\rm d}\beta}{(16\pi)^3} \, |\chi_\lambda(\beta, \mathbf{k}_\perp, \lambda_1, \lambda_2)|^2 \delta(\alpha - \beta), \tag{34}$$

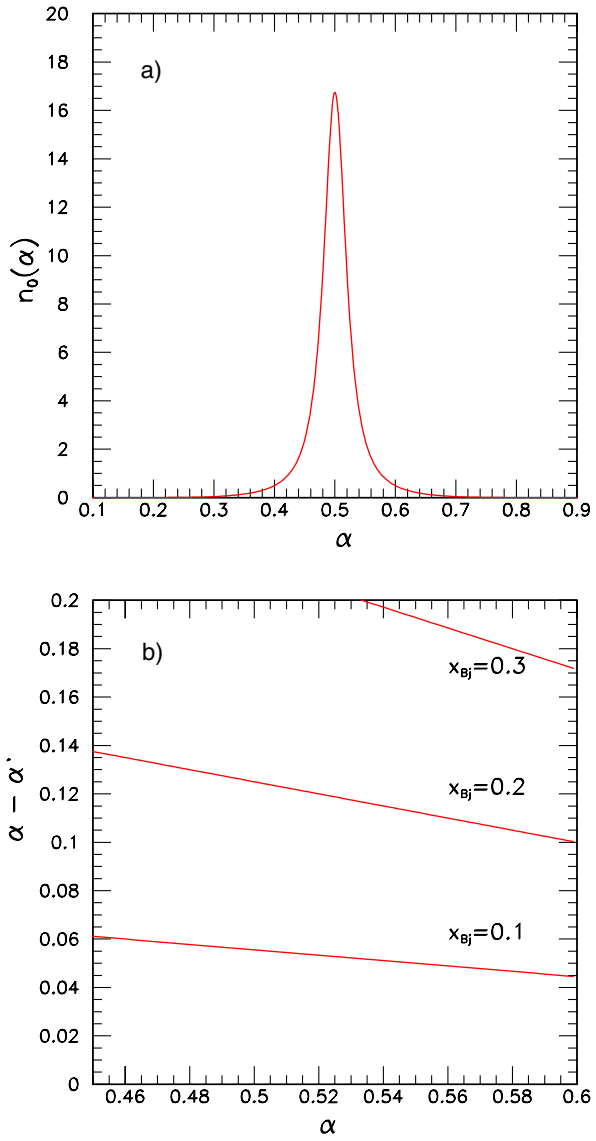

Fig. 3. (a) Longitudinal momentum distribution of the nucleon within the deuteron. (b) Gap between the fractions of longitudinal momentum carried by the active nucleon before and after the interaction as a function of $\xi(x_{\rm Bj})$ and α.

which is normalized according to

$$\int {\rm d}\alpha \; n_\lambda(\alpha) = 1. \tag{35}$$

In fig. 3a we show $n_0(\alpha)$ evaluated with the wave function from the Paris potential [12]. This distribution is strongly peaked at $\alpha = 0.5$ and its width is of the order of the ratio of the binding energy divided by the nucleon mass.

In the impulse approximation, the active nucleon after the interaction with the photon carries a fraction of longitudinal momentum which is given by

$$\alpha' = \alpha - \frac{x_{\rm Bj}}{1 - x_{\rm Bj}}(1 - \alpha) \quad . \tag{36}$$

In fig. 3b we plot the difference $\alpha - \alpha'$ as a function of α and for several values of the skewness. We see that for $x_{\rm Bj} > 0.1$ this difference is larger than the width of the momentum distribution, and therefore, we will inevitably have a too fast or too slow nucleon (in the longitudinal direction). In this case, the central region of momentum, where a maximal contribution is expected, is missed and then the cross-sections will decrease very fast with $x_{\rm Bj}$. In other words, there is an increasing difficulty in forming a coherent final state as the longitudinal momentum transfer, *i.e.* $x_{\rm Bj}$, increases. In that case, other coherent mechanisms, which could involve higher Fock-space components, will presumably become dominant. Not much is known about these states, but it should be emphasized that the suppression of the diagram of fig. 1 occurs at $x_{\rm Bj}$ as low as 0.2, so that there is room to check the importance of the contribution of these "exotic" states.

The choice of the nucleon GPDs deserves a more detailed discussion.

4.2 Modelling nucleon GPDs

Let us first consider the helicity-conserving nucleon GPDs. Following [13], we have taken a factorized ansatz for the t-dependence of the nucleon GPDs:

$$H^u(x_N,\xi_N,t) = h^u(x_N,\xi_N)\frac{1}{2}F_1^u(t), \tag{37}$$

$$H^d(x_N,\xi_N,t) = h^d(x_N,\xi_N)F_1^d(t), \tag{38}$$

$$\tilde{H}^q(x_N,\xi_N,t) = \tilde{h}^q(x_N,\xi_N)\tilde{F}^q(t), \tag{39}$$

and neglected the strange-quark contributions H^s. The flavour decomposition of the proton and neutron Dirac form factor, for which we have taken the usual dipole parameterizations [14], gives

$$F_1^u(t) = 2F_1^p + F_1^n, \tag{40}$$

$$F_1^d(t) = 2F_1^n + F_1^p. \tag{41}$$

For the axial form factor we have taken $\tilde{F}^q(t) = (1 - t/M_{\rm A}^2)^{-2}$ with $M_{\rm A} = 1.06$ GeV [15]. For h^q and $\tilde{h}^q$ we follow the ansatz based on double distributions:

$$h^q(x_N,\xi_N) = \int_0^1 {\rm d}x' \int_{-1+x'}^{1-x'} {\rm d}y' \,[\delta(x_N - x' - \xi_N y')\, q(x') - \delta(x_N + x' - \xi_N y')\, \bar{q}(x')\,]\, \pi(x',y'), \tag{42}$$

$$\tilde{h}^q(x_N,\xi_N) = \int_0^1 {\rm d}x' \int_{-1+x'}^{1-x'} {\rm d}y'\, \delta(x_N - x' - \xi_N y') \cdot \Delta q_V(x')\, \pi(x',y'), \tag{43}$$

$$\pi(x',y') = \frac{3}{4}\,\frac{(1-x')^2 - y'^2}{(1-x')^3}, \tag{44}$$

where we have only considered the polarization of the valence quarks. To avoid numerical problems with the integrals in the low-x region, we have followed the procedure explained in [8]. Throughout this work we have taken the parameterization MRST 2001 NLO [16] for the unpolarized parton distributions and the parameterization LSS01 [17] for the polarized ones.

Concerning the helicity flip nucleon GPDs, E^q and $\tilde{E}^q$, we can safely neglect the latter since we deal with an isoscalar target. The former is suppressed in the $V_{\lambda'\lambda}$ amplitudes, eq. (28), by kinematical factors. However, one might think that there could be physical situations which could be sensitive to this GPD: in the amplitudes where $\lambda' \neq \lambda$ the transition with $H^{\rm IS}$ is done at the cost of using the D-wave of the deuteron, *i.e.*, by making use of angular momentum. The term with $E^{\rm IS}$ could flip the helicity at the nucleon level and, therefore, the (rather small) D-wave admixture in the deuteron is not necessary.

Unfortunately, most of the observables are dominated by amplitudes with $\lambda' = \lambda$. We have checked that effects due to $E^{\rm IS}$ are negligible and we have only shown how tiny they are for the sum rules, just for illustrative purposes. Furthermore, when modelling E^q following the steps explained in [13], one realizes that the isoscalar combination is suppressed. Recall that E^q is normalized to the Pauli form factor, that in the forward limit gives just the anomalous magnetic moment, very small for the isoscalar case.

Let us stress that the available models of GPDs are fraught with uncertainties, in particular in the ERBL region. There, GPDs describe the emission of a $q\bar{q}$ pair from the target, and an ansatz only using the information from usual parton densities should be used with care. Notice also that, while for $x > \xi$ GPDs are bounded from above [18], no analogous constraints are known in the ERBL region. A particular type of contribution in the ERBL region is the Polyakov-Weiss D-term [19], which we will not include in our analysis.

4.3 Results

With the ingredients mentioned before we plot in figs. 4 and 5 the corresponding generalized quark distributions, which are flavorblind for the deuteron case. The support of these functions is $-1 < x < 1$, but we have plotted only the central region. In addition, due to the assumption made when modelling $\tilde{H}$ for the nucleon (the non-contribution of the polarized sea) we have that $\tilde{H}_i(x \leq \xi, \xi, t)$ vanishes.

The rapid falloff of the GPDs with x reflects the fact that the impulse approximation, *i.e.*, the single-nucleon contribution, cannot account for very large longitudinal momentum.

Notice also the huge differences in the scales of the various GPDs: for the vector sector, H_3 dominates over the others, whereas H_4 or H_5 are very small. The respective sizes may be related to the values of the different deuteron form factors for the GPDs that have a sum-rule connection to them (see eq. (5)).

The form factors that we have used in the current (G_1, G_2, G_3) are related with the usual charge monopole, $G_{\rm C}$, magnetic dipole, $G_{\rm M}$ and charge quadrupole, $G_{\rm Q}$ in

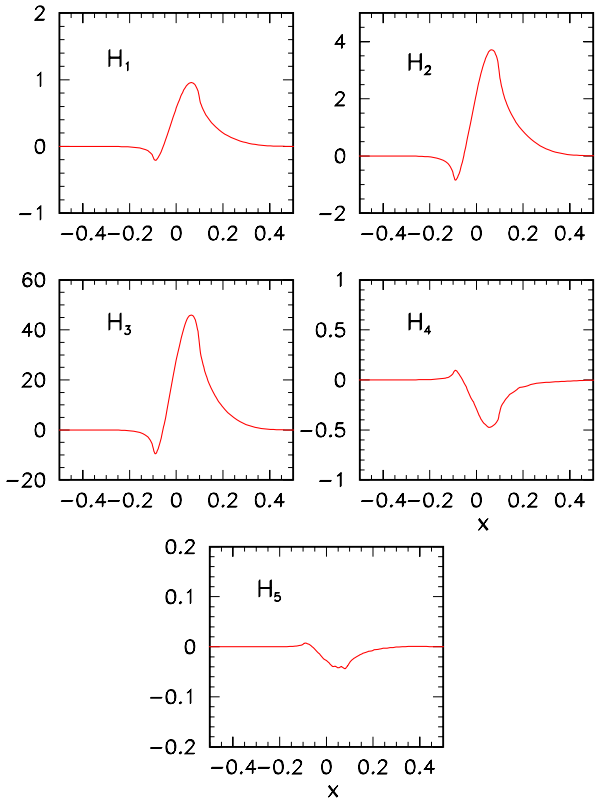

Fig. 4. Generalized quark distributions for the deuteron at $Q^2 = 2$ GeV^2, $\xi = 0.1$ and $t = -0.25$ GeV^2.

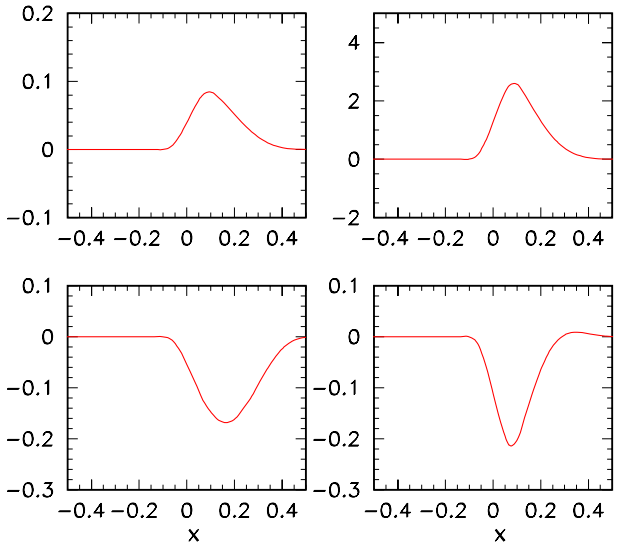

Fig. 5. Generalized polarized quark distributions for the deuteron at $Q^2 = 2$ GeV^2, $\xi = 0.1$ and $t = -0.25$ GeV^2. $\tilde{H}_1$ (upper left), $\tilde{H}_2$ (upper right), $\tilde{H}_3$ (lower left), $\tilde{H}_4$ (lower right).

the following way:

$$
\begin{aligned}
G_1(t) &= G_{\rm C}(t) - \frac{2}{3}\eta G_{\rm Q}(t)\,, \\
G_2(t) &= G_{\rm M}(t)\,, \\
(1+\eta)G_3(t) &= G_{\rm M}(t) - G_{\rm C}(t) + \left(1+\frac{2}{3}\eta\right) G_{\rm Q}(t)
\end{aligned}
\tag{45}
$$

with $\eta = \frac{-t}{4M^2}$. With the flavour decomposition of the form factors for the deuteron, we have $G_i^u = G_i^d \equiv G_i^q = 3G_i$. The dominant form factor is G_3^q due mainly to the size of $G_{\rm Q}(t)$ (see [20]), and if we consider the form factors as a normalization condition for the GPDs, it is natural that H_3 dominates over the other GPDs.

Notice, however, that the fact that a GPD is large does not mean necessarily that it plays a major role in the observables: it has to be multiplied by the corresponding kinematical coefficients.

It is worthwhile mentioning that we have plotted the GPDs at a particular value of $-t$, *i.e.* we cannot set $t = 0$ to study the ξ and x behaviour. The reason is that, even if we assume a factorized form for the t-dependence in the nucleon, in the deuteron we cannot isolate this t-dependence. In fact, there are two sources of t-dependence in H_i and $\tilde{H}_i$: first, the explicit t-dependence in the nucleon GPDs and, secondly, the most important source, the transverse momentum in the deuteron wave function. Then, we cannot circumvent the kinematical relationship between ξ and t, eq. (12), and for a non-vanishing ξ we have inevitably a non-vanishing t.

4.4 Sum rules: tests and discussions

In the impulse approximation we have retained only the lowest Fock-space state of the deuteron (figs. 2a and b). As we can see, the $q\bar{q}$ components which are tested in the region $|x| < \xi$, are considered only within the nucleon itself (fig. 2b).

We have also neglected the $N\bar{N}$ components in the deuteron wave function, which could give rise to diagrams like the one in fig. 2c. When one evaluates the elastic deuteron form factor [21,22], this is an exact approximation since one can always choose a frame where the momentum transfer is purely transverse and in that case, $\Delta^+ = 0$ and no pairs can be created from or annihilated into a photon.

In the DVCS and DEMP cases, there is a non-vanishing momentum transfer in the longitudinal direction, controlled by the skewness parameter ξ. Therefore, there are necessarily diagrams where the final photon goes out from the annhilation of, for example, a $N\bar{N}$ pair or a $q\bar{q}$ (see fig. 2c). One has to include these higher Fock-space components to recover Lorentz invariance.

Lorentz invariance is the physical reason why the sum rules (5), obtained by integrating the GPDs over x, become ξ-independent. When we perform that integration we have matrix elements of local operators (form factors) that cannot depend on the artifacts of the kinematics, *i.e.* of the separation between transverse and longitudinal momentum transfer (see [23] for a more detailed discussion on this point).

We can make use of this relationship between the ξ-independence of the sum rules and the contribution of higher Fock-space states in the deuteron to check how accurate the impulse approximation is. We have plotted in

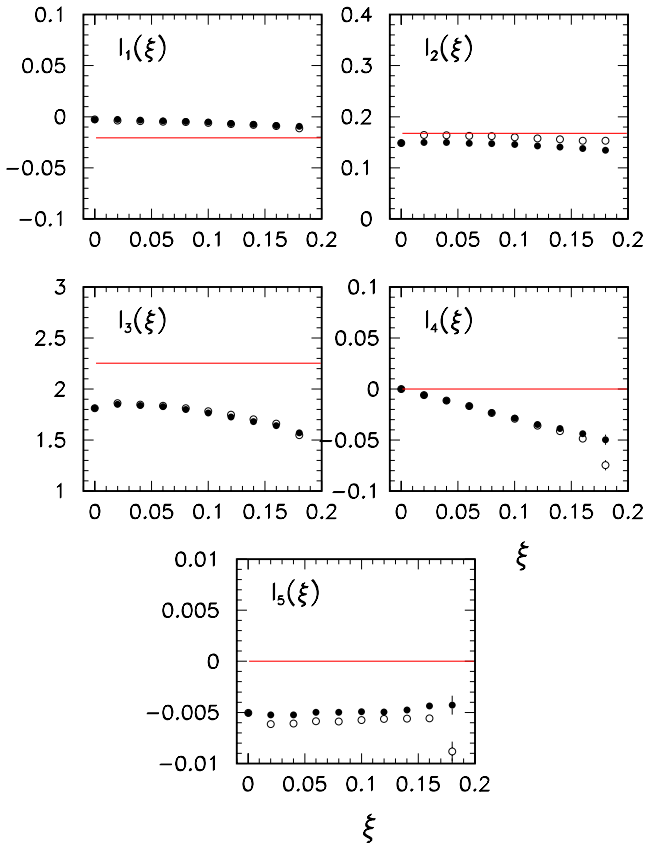

Fig. 6. Sum rules for the vector GPDs at $Q^2 = 2$ GeV^2 and $t = -0.5$ GeV^2. Solid lines are the expected theoretical result and points are the results obtained with our model. Filled points: the nucleon GPD $E^{\rm IS}$ is not included; empty points: $E^{\rm IS}$ included.

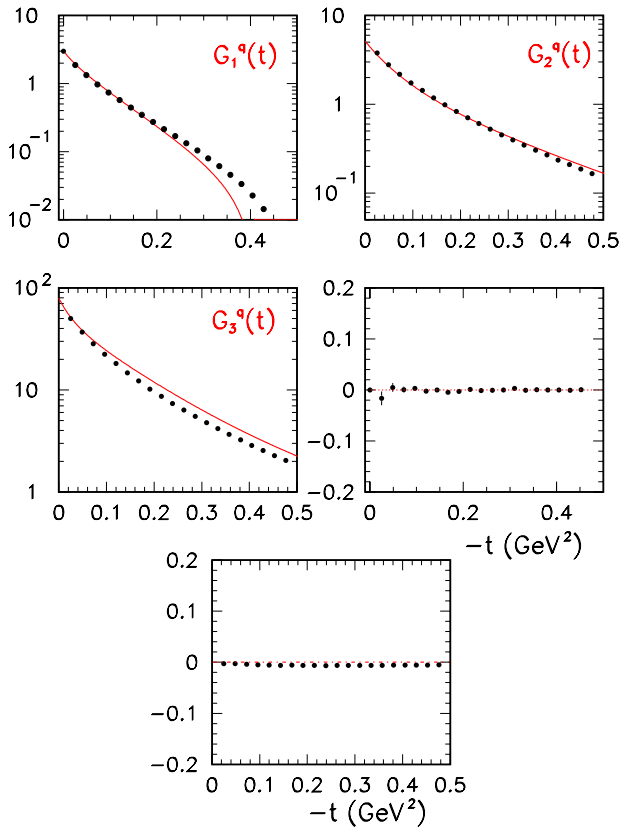

Fig. 7. Sum rules for the vector GPDs at $Q^2 = 2$ GeV^2 and fixed $\xi = 0$ as a function of t. Solid lines represent the expected theoretical values whereas points are the results of our evaluation.

fig. 6 the quantities

$$I_i(\xi) = \int_{-1}^{1} {\rm d}x H_i^q(x,\xi,t). \qquad (46)$$

For a fixed t, the functions $I_i(\xi)$ would be constant if the impulse approximation were exact: straight lines in the figure show the "theoretical" values of the sum rule according to the experimental parameterization of the form factors. Any residual ξ-dependence of $I_i(\xi)$ is a measure of the importance of the higher Fock-space states that we have not included in our description. Looking at this figure and to the corresponding one for the axial case, we can see that this dependence is fairly mild, which indicates that, in the kinematical regime that we are interested in, the deuteron is essentially a two-nucleon state[2]. As ξ increases, the impulse approximation would become a too rough approximation with respect to Lorentz invariance.

One should distinguish between the variation in ξ of the quantities $I_i(\xi)$ and the particular values they take, which are sensitive also to the details of the employed model. In fig. 6 we see that the points obtained with our calculations are quite close to the experimental parameterization. Obviously, the models works better at smaller ξ, for the reasons exposed above. In fact, in fig. 7, we show the t-dependence of the sum rules at $\xi = 0$, where it is clearly seen that results agrees quite well with the experimental parameterization, when available, or with the values imposed by time reversal or Lorentz invariance. This comes as no surprise, since it is well known that the light-cone deuteron wave function is able to give the deuteron form factors at the momentum transfer we are working (see [24] for a recent review). In the context of our discussion, at $\xi = 0$ the pair creation or annihilation with the photon vanishes in the light-cone formalism. In fig. 8, we plot the same quantities (eq. (46)) for the axial-vector GPDs.

One final remark concerns also the subtleties of the light-cone formalism: nucleons are on-shell, *i.e.*, they verify, with the notation employed in the previous section, that

$$p_i^- = \frac{m^2 + \mathbf{p}_{i_\perp}^2}{2p_i^+}. \qquad (47)$$

But, they are off light-cone energy shell, and, as a consequence, if $P^+ = p_1^+ + p_2^+$ and $\mathbf{P}_\perp = \mathbf{p}_{1\perp} + \mathbf{p}_{2\perp}$ (as it is the case), one has that $P^- \neq p_1^- + p_2^-$. Therefore, one has

[2] We checked that the inclusion of the nucleon GPD $E^{\rm IS}$ does not introduce any improvement at all: its contribution vanishes exactly at $\xi = 0$, and is always small at other values of ξ.

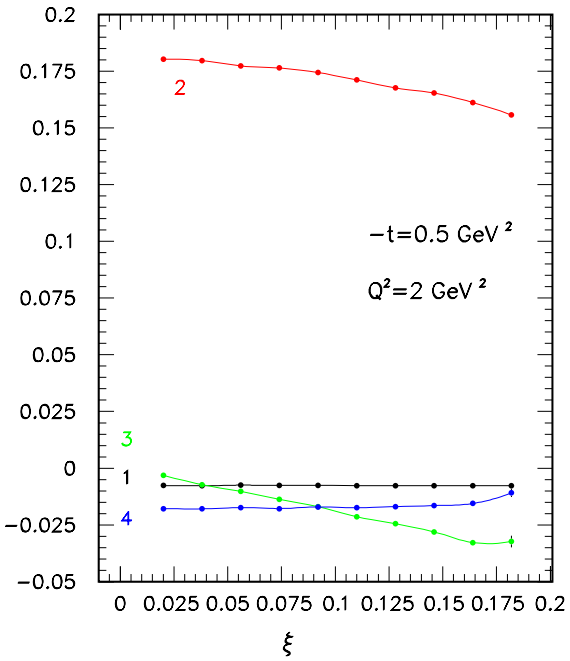

Fig. 8. Sum rules for the axial-vector GPDs at $Q^2 = 2$ GeV^2 and $t = -0.5$ GeV^2.

that the momentum transfer t defined from the deuteron variables does not coincide with the one defined from the variables of the active nucleon. Moreover, the upper limit over ξ_N^2 is not $\frac{-t}{4m^2-t}$. If, nevertheless, one enforces ξ_N^2 to have this upper limit, this leads only to a tiny shift in the value of $\alpha_{\min}$ in the integrals. From the practical point of view, these differences are too tiny to be seen in the numerical calculation, unless one goes to very large values of $-t$. This just reflects the fact that the off-shellness effects in the light-cone energy are of the order of the binding energy over the longitudinal momentum [25]:

$$P^- - (p_1^- + p_2^-) \propto \frac{V}{P^+} \tag{48}$$

and in our case this is of the order of the binding energy of the deuteron over the center-of-mass energy, *i.e.*, very small.

5 DVCS amplitudes and cross-sections

There are two processes that contribute to the deeply virtual Compton scattering amplitude of eq. (1) under consideration. The first one is the Bethe-Heitler process where the outgoing photon is produced from the lepton line. Its amplitude (for either electrons or positrons) is given by

$$T_{\rm BH} = -\frac{e^3}{t}\,\epsilon^*_\mu(\mathbf{q}',\lambda')j_\nu(0)L^{\mu\nu}, \tag{49}$$

where e is the proton charge. The deuteron current is given by

$$\begin{aligned} j_\mu = &- G_1(t)(\epsilon'^*\cdot\epsilon)2\bar{P}_\mu + G_2(t)\left[(\epsilon'^*\cdot 2\bar{P})\epsilon_\mu + (\epsilon\cdot 2\bar{P})\epsilon'^*_\mu\right] \\ &- G_3(t)(\epsilon'^*\cdot 2\bar{P})(\epsilon\cdot 2\bar{P})\frac{\bar{P}_\mu}{M^2}, \end{aligned} \tag{50}$$

where the three form factors have been measured in the low- and medium-momentum transfer ranges [20]. The leptonic tensor $L^{\mu\nu}$ is given by

$$L^{\mu\nu} = \bar{u}(\mathbf{k}',h')\left[\gamma^\mu\frac{1}{(\not{k}+\not{q}')}\gamma^\nu + \gamma^\nu\frac{1}{(\not{k}-\not{q}')}\gamma^\mu\right]u(\mathbf{k},h). \tag{51}$$

The Bethe-Heitler process is thus completely known in terms of already measured form factors.

The second process where the photon is emitted from the hadronic part is more interesting in terms of the study of the hadronic structure. It is called virtual Compton scattering since it can be decomposed in a $\gamma^* A \to \gamma B$ process. Its amplitude $T_{\rm VCS}$ is written as

$$T_{\rm VCS} = \pm\frac{e^3}{Q^2}\sum_\lambda \Omega(h,\lambda)M_{H'\lambda',H\lambda}, \tag{52}$$

where the upper sign is for electrons and the lower one for positrons and the function Ω comes from the decomposition of the leptonic current in terms of the polarization vector of the virtual photon,

$$\bar{u}(\mathbf{k}',h)\gamma^\nu u(\mathbf{k},h) = \sum_\lambda \frac{Q}{\sqrt{1-\epsilon}}\tilde{\Omega}(h,\lambda)\epsilon^\nu(\mathbf{q},\lambda), \tag{53}$$

$$\tilde{\Omega}(h,\lambda) = \left[\delta_{\lambda 0}\sqrt{2\epsilon} - \frac{\lambda}{\sqrt{2}}(\sqrt{1+\epsilon}+2h\lambda\sqrt{1-\epsilon})e^{-i\lambda\phi}\right].$$

Sometimes we will also use

$$\Omega(h,\lambda) \equiv \frac{Q}{\sqrt{1-\epsilon}}\tilde{\Omega}(h,\lambda). \tag{54}$$

The photon-deuteron helicity amplitudes are defined as

$$M_{H'\lambda',H\lambda} = \epsilon^*_\mu(\mathbf{q}',\lambda')\epsilon_\nu(\mathbf{q},\lambda)H^{\mu\nu} \tag{55}$$

and

$$\begin{aligned} H^{\mu\nu} = &(g^{\mu\nu} - \tilde{p}^\mu\tilde{n}^\nu - \tilde{n}^\mu\tilde{p}^\nu) \\ &\cdot\int_{-1}^{1}{\rm d}x\left(\frac{1}{x-\xi+i\eta}+\frac{1}{x+\xi-i\eta}\right)\sum_q e_q^2 V^q_{\lambda'\lambda} \\ &+i\epsilon^{\mu\nu\alpha\beta}\tilde{p}_\alpha\tilde{n}_\beta \\ &\cdot\int_{-1}^{1}{\rm d}x\left(\frac{1}{x-\xi+i\eta}-\frac{1}{x+\xi-i\eta}\right)\sum_q e_q^2 A^q_{\lambda'\lambda} \end{aligned} \tag{56}$$

with the convention $\epsilon_{0123} = +1$.

For completeness, let us first write down the formula for the cross-section of the Bethe-Heitler process on the deuteron

$$\overline{\sum}|T_{\rm BH}|^2 = \frac{(4\pi\alpha_{\rm em})^3}{t^2}[\mathcal{K}_A A(t) + \mathcal{K}_B B(t)], \tag{57}$$

where A, B are the elastic structure functions of the deuteron, which are well known in the low-momentum region, and the kinematical coefficients are:

$$\mathcal{K}_B = -\frac{2M^2}{(k\cdot q')(k'\cdot q')}[(2(k\cdot q')+t)^2+(2(k\cdot q')+Q^2)^2],$$
$$\mathcal{K}_A = -\mathcal{K}_B + \frac{4t}{(k'\cdot q')}(M^2+s+Q^2-2s_{kp}) + \frac{t}{2(k\cdot q')(k'\cdot q')}\{(2M^2+Q^2-2s_{kp})^2-(Q^2-2t)^2 + 4(Q^2+s-s_{kp})^2+4t(t+s-s_{kp})\} \quad (58)$$

with $s_{kp} = (k+p)^2$.

The VCS amplitude gives a contribution to the cross-section which may be decomposed in terms of its azimuthal dependence as

$$\overline{\sum}|T_{\rm VCS}|^2 = \frac{1}{3}\frac{(4\pi\alpha_{\rm em})^3}{Q^2(1-\epsilon)}\sum_{H,H'}\big(2|M_{H'1,H1}|^2 + 2|M_{H'1,H-1}|^2 + 4\epsilon|M_{H'1,H0}|^2 + 4\sqrt{\epsilon(1+\epsilon)}\,\cos\phi\,{\rm Re}[M_{H'1,H0}M^*_{H'1,H-1} - M_{H'1,H0}M^*_{H'1,H1}] - 4\epsilon\cos(2\phi){\rm Re}[M_{H'1,H-1}M^*_{H'1,H1}]\big). \quad (59)$$

The interference between the two processes leads to a contribution to the DVCS cross-section which may be written as

$$\overline{\sum}\;(T_{\rm VCS}T^*_{\rm BH}+T^*_{\rm VCS}T_{\rm BH}) = \mp\frac{2}{3}\frac{(4\pi\alpha_{\rm em})^3}{Qt\sqrt{1-\epsilon}} \cdot \sum_{H,H',\lambda,h} 2h\;{\rm Re}[\epsilon^*_\mu(\mathbf{q}',\lambda'=+1)j_\nu L^{\mu\nu}\tilde{\Omega}(h,\lambda)] \cdot {\rm Re}[M_{H'1,H\lambda}], \quad (60)$$

where the upper sign stands for electrons and the lower one for positrons.

The study of the initial electron helicity dependence may be expressed through the following weighted contributions to the cross-section:

$$\overline{\sum}2h|\;\;T_{\rm BH}|^2 = 0, \quad (61)$$

$$\overline{\sum}2h|T_{\rm VCS}|^2 = \frac{4}{3}\frac{(4\pi\alpha_{\rm em})^3}{Q^2}\sqrt{\frac{\epsilon}{1-\epsilon}} \cdot \sum_{H,H'}\sin\phi\;{\rm Im}[M_{H'1,H0}M^*_{H'1,H1} - M_{H'1,H0}M^*_{H'1,H-1}], \quad (62)$$

$$\overline{\sum}2h\,(T_{\rm VCS}T^*_{\rm BH}+T^*_{\rm VCS}T_{\rm BH}) = \mp\frac{2}{3}\frac{(4\pi\alpha_{\rm em})^3}{Qt\sqrt{1-\epsilon}} \cdot \sum_{H,H',\lambda,h} 2h\;{\rm Im}[\epsilon^*_\mu(\mathbf{q}',\lambda'=+1)j_\nu L^{\mu\nu}\tilde{\Omega}(h,\lambda)] \cdot {\rm Im}[M_{H'1,H\lambda}], \quad (63)$$

where the upper sign stands for electrons and the lower one for positrons.

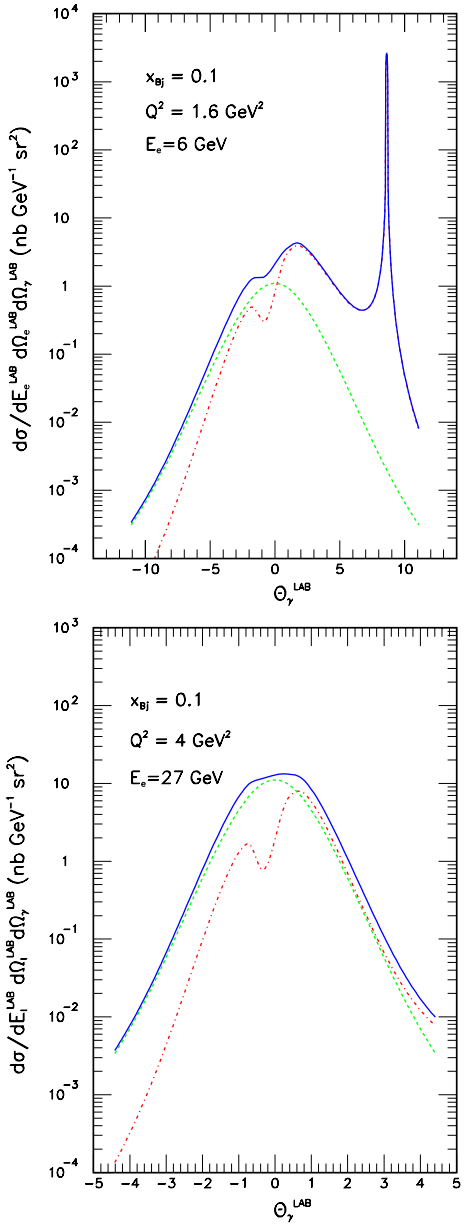

Fig. 9. Unpolarized differential cross-section for DVCS for typical kinematics at JLab (top panel) and HERMES (bottom panel). Dashed-dotted line: BH only; dashed line: DVCS only; full line: BH + DVCS + interference.

6 Numerical results for DVCS

Our model enables us now to estimate the cross-section of coherent deeply virtual Compton scattering on the deuteron. We are particularly interested in the forthcoming experiments at JLab and Hermes at DESY, and we thus shall present results for the kinematics of these experimental set-ups.

We present in fig. 9 the unpolarized cross-section for low- (left panel) and medium- (right panel) energy reactions. The Bethe-Heitler and VCS contributions are shown as well as their interference. The relative importance of these contributions depends much on the production an-

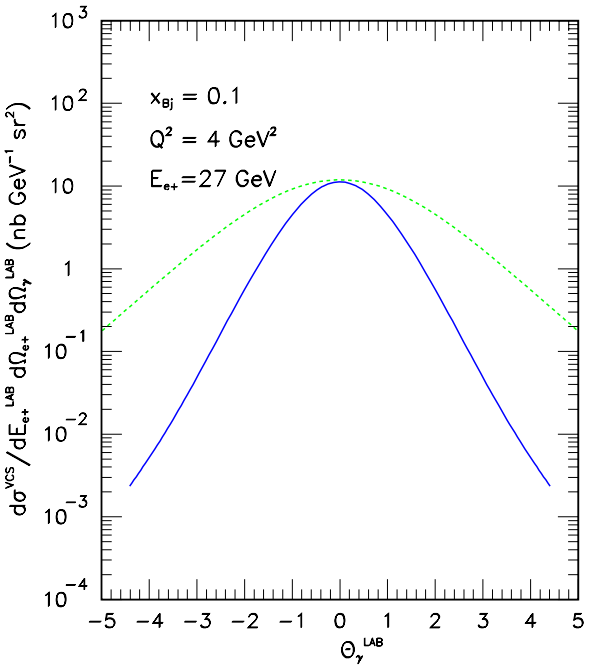

Fig. 10. Comparison of the DVCS cross-sections on a proton (dashed line) and deuteron (solid line) target for $x_{\rm Bj} = 0.1$ in the deuteron case (respectively, 0.2 for the proton), $Q^2 = 4$ GeV^2 and $E_{e^+} = 27$ GeV.

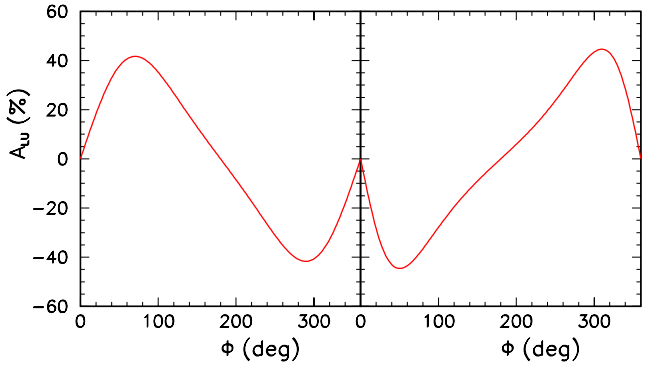

Fig. 11. Azimuthal dependence of the beam spin asymmetry as defined in the text. Left: $x_{\rm Bj} = 0.2$, $Q^2 = 2$ GeV^2 and $E_e = 6$ GeV. Right: $x_{\rm Bj} = 0.1$, $Q^2 = 4$ GeV^2 and $E_{e^+} = 27$ GeV. In both cases t is fixed to -0.3 GeV^2.

gle of the final photon, as can be read from the figure. To discuss the feasibility of the experiment, a comparison to the proton target case is welcome. This is shown in fig. 10 for medium-energy reactions.

Coherent deep VCS is certainly not a negligible effect at small values of t and we can expect that this process should soon become observable so that some knowledge of the deuteron GPDs will become accessible. More than testing the validity of the impulse approximation, the goal of such an experiment is to observe some definite deviation from the impulse approximation predictions, thereby indicating some non-trivial short-distance content of the deuteron. To scrutinize such effects, it is interesting to

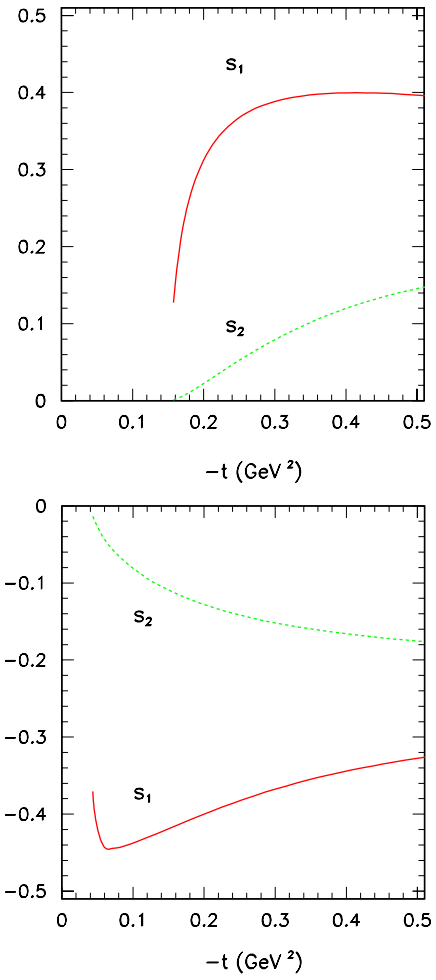

Fig. 12. Coefficients of the Fourier decomposition of the beam spin asymmetry: $A_{LU} = a_0 + s_1 \sin\phi + s_2 \sin 2\phi$ as a function of t. Values of $x_{\rm Bj}$, Q^2 and E_l as in fig. 11.

turn to some more specific observables, such as spin and charge asymmetries.

The beam spin asymmetry is defined as

$$A_{LU}(\phi) = \frac{{\rm d}\sigma^{\uparrow}(\phi) - {\rm d}\sigma^{\downarrow}(\phi)}{{\rm d}\sigma^{\uparrow}(\phi) + {\rm d}\sigma^{\downarrow}(\phi)}, \tag{64}$$

where ϕ is the angle between the lepton and hadron scattering planes. The numerator is proportional to the interference between the Bethe-Heitler and the VCS amplitudes.

Our predictions calculated with our modelized deuteron GPDs are shown in fig. 11 for JLab and Hermes energies. The sign of the asymmetry is reversed for a positron beam. Such a sizable asymmetry should be quite easily measured. It will constitute a crucial test of the validity of any model.

It has been shown [2] that, asymptotically, the beam spin asymmetry exhibits a $\sin(\phi)$ azimuthal dependence. We have performed a Fourier decomposition of the asymmetry A_{LU} obtained for the deuteron and, indeed, we have checked the dominance of the $\sin(\phi)$ component, even at

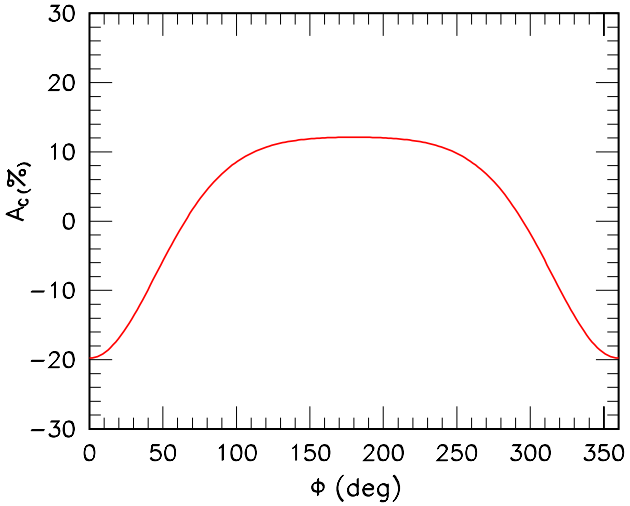

Fig. 13. Azimuthal dependence of the beam charge asymmetry A_C for the kinematics of HERMES shown in previous figures.

relatively low values of Q^2. But we also have a sizeable $\sin(2\phi)$ component (see fig. 12), which is less suppressed than in the nucleon case. This is likely to come from the following fact: the Bethe-Heitler propagators exibit when $t \neq t_0$ an azimuthal dependence in $\cos(\phi)$ which goes with terms of the order of t/Q^2, but also with terms of the order m^2/Q^2. In the nucleon case this $\sin(2\phi) = 2\sin(\phi)\cos(\phi)$ component was already seen [5] under some kinematical conditions, and the larger deuteron mass enhances it. In that respect, we expect that the scaling regime signed by the dominance of the $\sin(\phi)$ component [2] is likely to be reached later in the deuteron case than in the proton case.

The beam charge asymmetry

$$A_C(\phi) = \frac{\mathrm{d}\sigma^{e^+} - \mathrm{d}\sigma^{e^+}}{\mathrm{d}\sigma^{e^+} + \mathrm{d}\sigma^{e^+}} \tag{65}$$

is also proportional to the interference of the Bethe-Heitler and the VCS processes. Its characteristic azimuthal dependence is shown in fig. 13. Its size is large enough for a feasible experimental evaluation.

7 Deep exclusive meson electroproduction

Deep exclusive meson electroproduction [26] may be discussed along the same lines as the DVCS reaction. The same QCD factorization property exists which allows to separate a short-distance subprocess from long-distance matrix elements, provided the initial virtual photon is longitudinally polarized. The same GPDs appear in principle in the deuteron sector, but selection rules select some of the GPDs. The meson production is described within the well-established colinear approximation [27] through the introduction of a distribution amplitude $\Phi(z, Q^2)$ which is generally parameterized through its asymptotic (in the sense of its Q^2 evolution) expression,

$$\Phi^\rho(z, Q^2) = 6 f^\rho z(1-z) \tag{66}$$

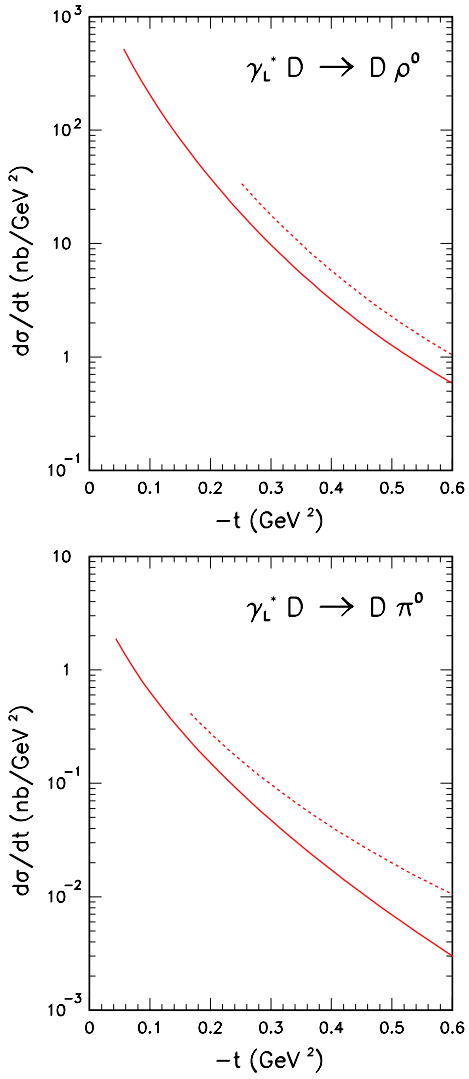

Fig. 14. ρ^0 (top) and π^0 (bottom) virtual photoproduction cross-sections at $x_{\mathrm{Bj}} = 0.1$, $Q^2 = 4$ GeV^2 (solid lines) and $x_{\mathrm{Bj}} = 0.2$, $Q^2 = 3$ GeV^2 (dashed lines).

for the ρ-meson, and

$$\Phi^\pi(z, Q^2) = 6\sqrt{2} f^\pi z(1-z) \tag{67}$$

for the π-meson, with $f^\rho = 216$ MeV and $f^\pi = 92$ MeV. The resulting amplitudes read (λ, λ' denoting deuteron polarizations as above):

$$\mathcal{M}^\rho_{\lambda',\lambda} = -ie\frac{16\pi\alpha_{\mathrm{S}}}{9}\frac{1}{Q}\int_0^1 \mathrm{d}z \frac{\Phi_\rho(z)}{z} \cdot \int_0^1 \mathrm{d}x \left(\frac{1}{x-\xi+i\epsilon} + \frac{1}{x+\xi-i\epsilon}\right)\frac{1}{\sqrt{2}} V^q_{\lambda',\lambda} \tag{68}$$

for the vector meson case, and

$$\mathcal{M}^\pi_{\lambda',\lambda} = -ie\frac{16\pi\alpha_{\mathrm{S}}}{9}\frac{1}{Q}\int_0^1 \mathrm{d}z \frac{\Phi_\pi(z)}{z} \cdot \int_0^1 \mathrm{d}x \left(\frac{1}{x-\xi+i\epsilon} + \frac{1}{x+\xi-i\epsilon}\right)\frac{1}{\sqrt{2}} A^q_{\lambda',\lambda} \tag{69}$$

for the pseudoscalar meson case, where the isosinglet nature of the deuteron has been used to simplify the results. The factor $\frac{1}{\sqrt{2}}$ in front of the matrix elements $V_{\lambda'\lambda}$ and $A_{\lambda'\lambda}$ come from the flavour decomposition of the ρ^0 and the π^0, *i.e.* $\frac{1}{\sqrt{2}}(|u\bar{u}\rangle - |d\bar{d}\rangle)$.

An interesting feature of meson electroproduction is the absence of a competing subrocess such as the Bethe-Heitler process in DVCS. Rates are also higher than in the DVCS case by a factor of $\alpha_{\rm S}/\alpha_{\rm em}$. The effective strong-coupling constant has been taken as $\alpha_{\rm S} = 0.56$ as advocated in [26]. Vector meson (mostly ρ^0) production selects the vector GPDs H^i, while pseudoscalar meson (mostly π^0) production selects the axial ones $\tilde{H}^i$. Meson pair production, described in the formalism of the generalized distribution amplitudes [28], may also be calculated in the same way.

We show in fig. 14 the prediction of our model for ρ^0 and π^0 electroproduction for $Q^2 = 4$ GeV^2, $x_{\rm Bj} = 0.1$ and for $Q^2 = 3$ GeV^2, $x_{\rm Bj} = 0.2$. As in the proton case, the vector meson production is enhanced with respect to the pseudoscalar meson production. The pseudoscalar production is quite small since the isosinglet nature of the deuteron forbids any enhanced $\tilde{E}$ contribution due to π^0 exchange in the t-channel.

8 Conclusion

We have demonstrated that deeply virtual Compton scattering and deep exclusive meson electroproduction on the deuteron is a feasible and promising field of study of the deuteron structure. More theoretical work is obviously needed before one can draw definite conclusions from forthcoming data. In particular, some of the so-called higher twist terms are needed [29] and should be estimated, at least those coming from target mass effects [30] that one may expect to be non-negligible. A first estimate of this effect has been given in the second reference of [9]. The inverse process, photoproduction of a lepton pair, sometimes called timelike Compton scattering, is also feasible, and should give complementary information as was shown in ref. [31] for the nucleon case. Double deeply virtual Compton scattering [32] may also be studied along the same lines. We expect that a deepened understanding of the short-distance structure of the deuteron will emerge from these studies.

We acknowledge useful discussions with M. Diehl, M. Garçon and F. Sabatie. Special thanks to P.A.M. Guichon and M. Vanderhaeghen for their help with technical calculations. This work was supported by the EC-IHP Network ESOP, Contract HPRN-CT-2000-00130.

Appendix A.

Appendix A.1. Light-cone deuteron wave function

We have chosen a covariant normalization for the one-particle states on the light cone:

$$\langle p'^+, \mathbf{p}'_\perp, \lambda' | p^+, \mathbf{p}_\perp, \lambda\rangle = (2\pi)^3 2p^+ \delta(p'^+ - p^+) \cdot \delta^{(2)}(\mathbf{p}'_\perp - \mathbf{p}_\perp)\delta_{\lambda\lambda'}, \quad \text{(A.1)}$$

where p^+ is defined in terms of the ordinary vector components as $p^+ = \frac{1}{\sqrt{2}}(p^0 + p^3)$ and $\mathbf{p}_\perp$ corresponds to the components in the transverse direction. We have to evaluate matrix elements of a quark operator between deuteron states, but eventually we have to deal with two quasi-free nucleon states. The definition of the state of a deuteron with momentum P and polarization λ in terms of two-nucleon state is

$$|P^+, \mathbf{P}_\perp, \lambda\rangle = \frac{1}{(16\pi)^3} \sum_{\lambda_1,\lambda_2} \int \frac{{\rm d}\xi_1}{\sqrt{\xi_1}} \frac{{\rm d}\xi_2}{\sqrt{\xi_2}}\, \delta(1-\xi_1-\xi_2) \cdot {\rm d}\mathbf{p}_{1_\perp} {\rm d}\mathbf{p}_{2_\perp} \delta^{(2)}(\mathbf{P}_\perp - \mathbf{p}_{1_\perp} - \mathbf{p}_{2_\perp}) \chi_\lambda(\xi_1, \mathbf{k}_{1_\perp}, \lambda_1; \xi_2, \mathbf{k}_{2_\perp}, \lambda_2) \cdot |p_1^+, \mathbf{p}_{1_\perp}, \lambda_1; p_2^+, \mathbf{p}_{2_\perp}, \lambda_2\rangle\,, \quad \text{(A.2)}$$

where $\xi_i = \frac{p_i^+}{P^+}$ and the transverse momenta $\mathbf{k}_{i_\perp}$ are the transverse momenta of the nucleons in a frame where $\mathbf{P}_\perp = 0$ (hadron frame). We have also kept the notation $\mathbf{p}_{i_\perp}$ to make explicit the fact that the states are defined in an arbitrary frame but the wave function always refers to the hadron frame. The relationship between both sets of coordinates is given by

$$\mathbf{k}_{i_\perp} = \mathbf{p}_{i_\perp} - \xi_i \mathbf{P}_\perp. \quad \text{(A.3)}$$

Let us define the measures that take part in the integrals as

$$[{\rm d}\xi] = {\rm d}\xi_1 {\rm d}\xi_2\, \delta(1-\xi_1-\xi_2), \quad \text{(A.4)}$$

$$[{\rm d}\mathbf{p}_\perp] = {\rm d}\mathbf{p}_{1_\perp} {\rm d}\mathbf{p}_{2_\perp}\, \delta^{(2)}(\mathbf{P}_\perp - \mathbf{p}_{1_\perp} - \mathbf{p}_{2_\perp}). \quad \text{(A.5)}$$

We can also perform the integrals over the transverse momenta in the hadron frame with the measure

$$[{\rm d}\mathbf{k}_\perp] = {\rm d}\mathbf{k}_{1_\perp} {\rm d}\mathbf{k}_{2_\perp}\, \delta^{(2)}(\mathbf{k}_{1_\perp} + \mathbf{k}_{2_\perp}). \quad \text{(A.6)}$$

The wave function of the deuteron with polarization λ is $\chi_\lambda(\xi_1, \mathbf{k}_{1_\perp}, \lambda_1; \xi_2, \mathbf{k}_{2_\perp}, \lambda_2)$ with λ_i being the polarization of the nucleons. It is normalized according to

$$\sum_{\lambda_1,\lambda_2} \int [{\rm d}\xi]\, [{\rm d}\mathbf{k}_\perp] |\chi_\lambda(\xi_1, \mathbf{k}_{1_\perp}, \lambda_1; \xi_2, \mathbf{k}_{2_\perp}, \lambda_2)|^2 = 1. \quad \text{(A.7)}$$

By taking advantage of the properties $\xi_1 \equiv \xi = 1 - \xi_2$ and $\mathbf{k}_{1_\perp} \equiv \mathbf{k}_\perp = -\mathbf{k}_{2_\perp}$, we can further simplify the notation in the wave function:

$$\chi_\lambda(\xi_1, \mathbf{k}_{1_\perp}, \lambda_1; \xi_2, \mathbf{k}_{2_\perp}, \lambda_2) \equiv \chi_\lambda(\xi, \mathbf{k}_\perp; \lambda_1, \lambda_2). \quad \text{(A.8)}$$

A last remark concerns the connection between the light-cone wave function of the deuteron and the ordinary (instant-form) relativistic wave function obtained with different phenomenological potentials. Whereas the first one is expressed in terms of light-cone coordinates, the latter one is a function of the ordinary three-vectors $\mathbf{k}_i$ and fulfills, in general, a Schrödinger-type equation. It can be

shown [33] that, if we define the longitudinal momentum from the light-cone coordinates as

$$k_z \equiv M_0(\xi - 1/2), \tag{A.9}$$

where M_0 is the free mass operator:

$$M_0^2 = \frac{m^2 + \mathbf{k}_\perp{}^2}{\xi(1-\xi)}, \tag{A.10}$$

then the eigenvalue equation fulfilled by $\chi_\lambda(\xi, \mathbf{k}_\perp; \lambda_1, \lambda_2)$ can be interpreted as a Schrödinger equation, and therefore, it can be related to the wave function obtained from phenomenological potentials in the instant-form formalism. More explicitly:

$$\chi_\lambda(\xi, \mathbf{k}_\perp; \lambda_1, \lambda_2) = \sum_{\mu_1,\mu_2} \left[\frac{M_0}{4\xi(1-\xi)}\right]^{1/2} \langle \lambda_1 | R_M^\dagger(\xi, \mathbf{k}_\perp) | \mu_1 \rangle \cdot \langle \lambda_2 | R_M^\dagger(1-\xi, -\mathbf{k}_\perp) | \mu_2 \rangle \, \chi_\lambda^{\mathrm{c}}(\mathbf{k}; \mu_1, \mu_2). \tag{A.11}$$

The global factor in the r.h.s. of the equation above is just the Jacobian of the transformation from the variables $\{\xi, \mathbf{k}_\perp\}$ to $\{\mathbf{k}\}$. We also have the matrix elements of the Melosh rotation, which relate the spin in the light front with the spin in the instant form of the dynamics. Finally, the (canonical) deuteron wave function $\chi_\lambda^{\mathrm{c}}(\mathbf{k}; \mu_1, \mu_2)$ is written as [34]

$$\chi_\lambda^{\mathrm{c}}(\mathbf{k}; \mu_1, \mu_2) = (16\pi^3)^{1/2} \sum_{L, m_L, m_s} \left(\frac{1}{2}\,\frac{1}{2}\,1 \,|\, \mu_1\, \mu_2\, m_s\right) \cdot (L\,1\,1\,|m_L\, m_s\, \lambda) Y_{L,m_L}(\hat{k}) u_L(k). \tag{A.12}$$

Appendix A.2. Helicity amplitudes and GPDs

We give here the kinematical coefficients that relate the helicity amplitudes evaluated with the light-cone helicity vectors and the generalized parton distributions. To be consistent with the choice of a right-handed set of polarization vectors made in [8], these expressions should be used only if $\Delta_x < 0$ in the explicit evaluation of $V_{\lambda',\lambda}$ or $A_{\lambda',\lambda}$.

By applying parity properties, we can reduce the number of independent helicity amplitudes $V_{\lambda',\lambda}$ down to five (that we have chosen to be V_{++}, V_{00}, V_{-+}, V_{0+}, V_{+0}) and to four in the pseudovector case $A_{\lambda',\lambda}$ (we keep A_{++}, A_{-+}, A_{0+}, A_{+0}). We recall these parity and time reversal properties:

$$V_{\lambda'\lambda} = (-1)^{\lambda'-\lambda} V_{-\lambda'-\lambda}, \tag{A.13}$$

$$A_{\lambda'\lambda} = -(-1)^{\lambda'-\lambda} A_{-\lambda'-\lambda}, \tag{A.14}$$

$$V_{\lambda'\lambda}(\xi) = (-1)^{\lambda'-\lambda} V_{\lambda\lambda'}(-\xi), \tag{A.15}$$

$$A_{\lambda'\lambda}(\xi) = (-1)^{\lambda'-\lambda} A_{\lambda\lambda'}(-\xi). \tag{A.16}$$

(A.17)

We set

$$H_i = \sum_{\lambda',\lambda} c_i^{\lambda'\lambda} V_{\lambda'\lambda}, \tag{A.18}$$

$$\tilde{H}_i = \sum_{\lambda',\lambda} \tilde{c}_i^{\lambda'\lambda} A_{\lambda'\lambda}, \tag{A.19}$$

where the sum covers only the helicity amplitudes that we have chosen as independent ones and the non-vanishing coefficients are:

$$\begin{aligned}
c_1^{++} &= \frac{1}{3(1-\xi^2)^2}(3\xi^4 - 7\xi^2 - 2D(1-\xi^2) + 2),\\
c_1^{00} &= \frac{1}{3(1-\xi^2)},\\
c_1^{-+} &= -\frac{1}{3D(1-\xi^2)^3}(2\xi^2 + D(3\xi^6 - 10\xi^4 + 9\xi^2 - 2)),\\
c_1^{0+} &= \frac{2}{3(1-\xi^2)^2}\sqrt{\frac{1+\xi}{2D(1-\xi)}}(D(1-\xi^2) + \xi),\\
c_1^{+0} &= -c_1^{0+}(\xi \to -\xi);
\end{aligned} \tag{A.20}$$

$$\begin{aligned}
c_2^{++} &= \frac{2}{1-\xi^2},\\
c_2^{-+} &= \frac{2\xi^2}{D(1-\xi^2)},\\
c_2^{0+} &= -\frac{1}{1-\xi}\sqrt{\frac{1+\xi}{2D(1-\xi)}},\\
c_2^{+0} &= -c_2^{0+}(\xi \to -\xi);
\end{aligned} \tag{A.21}$$

$$c_3^{-+} = -\frac{1}{D},$$

$$\begin{aligned}
c_4^{++} &= -\frac{2\xi}{1-\xi^2},\\
c_4^{-+} &= -\frac{2\xi}{D(1-\xi^2)^2},\\
c_4^{0+} &= \frac{1}{1-\xi}\sqrt{\frac{1+\xi}{2D(1-\xi)}},\\
c_4^{+0} &= c_4^{0+}(\xi \to -\xi);
\end{aligned} \tag{A.22}$$

$$\begin{aligned}
c_5^{++} &= -\frac{1}{(1-\xi^2)^2}(\xi^2 + 2D(1-\xi^2) + 1),\\
c_5^{00} &= \frac{1}{(1-\xi^2)},\\
c_5^{-+} &= -\frac{1}{D(1-\xi^2)^3}(2\xi^2 + D(1-\xi^4)),\\
c_5^{0+} &= \frac{2}{(1-\xi^2)^2}\sqrt{\frac{1+\xi}{2D(1-\xi)}}(D(1-\xi^2) + \xi),\\
c_5^{+0} &= -c_5^{0+}(\xi \to -\xi).
\end{aligned} \tag{A.23}$$

In the pseudovector case they are:

$$\begin{aligned}
\tilde{c}_1^{++} &= \frac{1}{(1+D(1-\xi^2))},\\
\tilde{c}_1^{-+} &= \frac{D(1-\xi^2)}{\xi(1+D(1-\xi^2))},\\
\tilde{c}_1^{0+} &= \frac{(1+\xi)\sqrt{2D(1-\xi^2)}}{2\xi(1+D(1-\xi^2))},\\
\tilde{c}_1^{+0} &= -\tilde{c}_1^{0+}(\xi\to-\xi);
\end{aligned} \tag{A.24}$$

$$\begin{aligned}
\tilde{c}_2^{++} &= \frac{1}{4(1+D(1-\xi^2))},\\
\tilde{c}_2^{-+} &= \frac{\xi^2-D(1-\xi^2)^2}{4D\xi(1-\xi^2)(1+D(1-\xi^2))},\\
\tilde{c}_2^{0+} &= -\frac{(1+\xi)}{4\xi\sqrt{2D(1-\xi^2)}(1+D(1-\xi^2))},\\
\tilde{c}_2^{+0} &= -\tilde{c}_2^{0+}(\xi\to-\xi);
\end{aligned} \tag{A.25}$$

$$\begin{aligned}
\tilde{c}_3^{++} &= -\frac{\xi}{4(1+D(1-\xi^2))},\\
\tilde{c}_3^{-+} &= -\frac{1}{4D(1-\xi^2)(1+D(1-\xi^2))},\\
\tilde{c}_3^{0+} &= \frac{(1+\xi)}{4\sqrt{2D(1-\xi^2)}(1+D(1-\xi^2))},\\
\tilde{c}_3^{+0} &= \tilde{c}_3^{0+}(\xi\to-\xi);
\end{aligned} \tag{A.26}$$

$$\begin{aligned}
\tilde{c}_4^{++} &= -\frac{1}{1-\xi^2},\\
\tilde{c}_4^{-+} &= -\frac{\xi}{D(1-\xi^2)^2},\\
\tilde{c}_4^{0+} &= \frac{1}{(1-\xi)\sqrt{2D(1-\xi^2)}},\\
\tilde{c}_4^{+0} &= -\tilde{c}_4^{0+}(\xi\to-\xi).
\end{aligned} \tag{A.27}$$

In the forward limit ($\xi\to 0, t\to 0$) we get the simplified expressions

$$H_1(x,0,0) = \frac{1}{3}(2V_{++}+V_{00}), \tag{A.28}$$

$$H_5(x,0,0) = (-V_{++}+V_{00}), \tag{A.29}$$

$$\tilde{H}_1(x,0,0) = A_{++}. \tag{A.30}$$

The integral over $H_1(x,0,0)$ is the parton number, which imposes a serious check on the construction of the helicity amplitudes in the forward limit.

Appendix A.3. Parameterization of the nucleon matrix elements

In a symmetric frame, where $\bar{P}^\mu = (p^\mu + p'^\mu)/2$ has no transverse momentum, we take the following parameterization:

$$\int \frac{\mathrm{d}\kappa}{2\pi} e^{i\kappa x}\ \langle p',\lambda'|\bar{\psi}_q\left(-\frac{\kappa}{2}\right)\gamma^+\psi_q\left(\frac{\kappa}{2}\right)|p,\lambda\rangle = \bar{u}(p',\lambda')\left[\gamma^+ H^q(x,\xi,t) + i\frac{\sigma^{+\alpha}\Delta_\alpha}{2m}E^q(x,\xi,t)\right]u(p,\lambda), \tag{A.31}$$

$$\int \frac{\mathrm{d}\kappa}{2\pi} e^{i\kappa x}\ \langle p',\lambda'|\bar{\psi}_q\left(-\frac{\kappa}{2}\right)\gamma^+\gamma_5\psi_q\left(\frac{\kappa}{2}\right)|p,\lambda\rangle = \bar{u}(p',\lambda')\left[\gamma^+\gamma_5 \tilde{H}^q(x,\xi,t) + \frac{\gamma_5\Delta^+}{2m}\tilde{E}^q(x,\xi,t)\right]u(p,\lambda), \tag{A.32}$$

where the integration path must be understood along the "−" direction. By using light-cone helicity states, which is close to the usual helicity in frames where the particle moves fast to the right and allows to get compact and elegant expressions, we have to insert in the previous equations the following results:

$$\begin{aligned}
&\bar{u}(p',\lambda')\gamma^+ u(p,\lambda) = 2\bar{p}^+\sqrt{1-\xi^2}\delta_{\lambda\lambda'},\\
&\bar{u}(p',\lambda')\gamma^+\gamma_5 u(p,\lambda) = 2\lambda 2\bar{p}^+\sqrt{1-\xi^2}\delta_{\lambda\lambda'},\\
&\bar{u}(p',\lambda')i\frac{\sigma^{+\alpha}\Delta_\alpha}{2m}u(p,\lambda) = 2\bar{p}^+\\
&\quad\cdot\left(-\frac{\xi^2}{\sqrt{1-\xi^2}}\,\delta_{\lambda\lambda'} + \frac{\sqrt{t_0-t}}{2m}\eta_\lambda\delta_{\lambda,-\lambda'}\right),\\
&\bar{u}(p',\lambda')\frac{\Delta^+}{2m}\gamma_5 u(p,\lambda) = 2\lambda 2\bar{p}^+\\
&\quad\cdot\left(-\frac{\xi^2}{\sqrt{1-\xi^2}}\,\delta_{\lambda\lambda'} + \xi\frac{\sqrt{t_0-t}}{2m}\eta_\lambda\delta_{\lambda,-\lambda'}\right),
\end{aligned} \tag{A.33}$$

where

$$\eta_\lambda = \frac{2\lambda\Delta_x - i\Delta_y}{|\boldsymbol{\Delta}_\perp|} \tag{A.34}$$

and $\Delta^\mu = p'^\mu - p^\mu$.

References

1. D. Müller, D. Robaschik, B. Geyer, F.M. Dittes, J. Hořejši, Fortsch. Phys. **42**, 101 (1994); X. Ji, Phys. Rev. Lett. **78**, 610 (1997); J. Phys. G **24**, 1181 (1998); A.V. Radyushkin, Phys. Rev. D **56**, 5524 (1997); J. Blümlein, B. Geyer, D. Robaschik, Nucl. Phys. B **560**, 283 (1999); A.V. Radyushkin, Phys. Rev. D **59**, 014030 (1999).
2. M. Diehl *et al.*, Phys. Lett. B **411**, 193 (1997).
3. P.A. Guichon, M. Vanderhaeghen, Prog. Part. Nucl. Phys. **41**, 125 (1998); A.V. Radyushkin hep-ph/0101225; X.D. Ji, J. Phys. G **24**, 1181 (1998); K. Goeke *et al.*, Prog. Part. Nucl. Phys. **47**, 401 (2001).
4. M. Burkardt, Phys. Rev. D **62**, 071503 (2000); J.P Ralston, B. Pire, Phys. Rev. D **66**, 111501 (2002); M. Diehl, Eur. Phys. J. C **25**, 223 (2002).
5. A. Airapetian *et al.*, Phys. Rev. Lett. **87**, 182001 (2001).

6. CLAS Collaboration (S. Stepanyan *et al.*), Phys. Rev. Lett. **87**, 182002 (2001).
7. J.C. Collins, L. Frankfurt, M. Strikman, Phys. Rev. D **56**, 2982 (1997); J. C. Collins, A. Freund, Phys. Rev. D **59**, 074009 (1999).
8. E.R. Berger, F. Cano, M. Diehl, B. Pire, Phys. Rev. Lett. **87**, 142302 (2001).
9. A. Kirchner, D. Müller, hep-ph/0202279; hep-ph/0302007; V. Guzey, M. Strikman, arXiv:hep-ph/0301216.
10. HERMES Collaboration (A. Airapetian *et al.*), arXiv:hep-ex/0302012; HERMES Collaboration (P. di Nezza, R. Fabbri), arXiv:hep-ex/0211008; t20 Collaboration (D. Abbott *et al.*), DAPNIA-SPHN-99-27.
11. F. Cano, B. Pire, Nucl. Phys. A **711**, 133 (2002); arXiv:hep-ph/0211444.
12. M. Lacombe *et al.*, Phys. Lett. B **101**, 139 (1981).
13. K. Goeke, M.V. Polyakov, M. Vanderhaeghen, Prog. Part. Nucl. Phys. **47**, 401 (2001).
14. S. Boffi *et al.*, Phys. Rep. **226**, 1 (1993).
15. L.A. Ahrens *et al.*, Phys. Rev. D **35**, 785 (1987).
16. A.D. Martin *et al.*, Eur. Phys. J. C **23**, 73 (2002).
17. E. Leader, A.V. Sidorov, D.B. Stamenov, Eur. Phys. J. C **23**, 479 (2002).
18. B. Pire, J. Soffer, O. Teryaev, Eur. Phys. J. C **8**, 103 (1999); P.V. Pobylitsa, Phys. Rev. D **65**, 077504; 114015 (2002).
19. M.V. Polyakov, C. Weiss, Phys. Rev. D **60**, 114017 (1999).
20. M. Garçon, J.W. Van Orden, Adv. Nucl. Phys. **26**, 294 (2001).
21. L.L. Frankfurt, M.I. Strikman, Nucl. Phys. B **148**, 107 (1979).
22. L.L. Frankfurt, T. Frederico, M. Strikman, Phys. Rev. C **48**, 2182 (1993).
23. S.J. Brodsky, M. Diehl, D.S. Hwang, Nucl. Phys. B **596**, 99 (2001).
24. J.R. Cooke, G.A. Miller, Phys. Rev. C **66**, 034002 (2002); J. R. Cooke, arXiv:nucl-th/0112029.
25. S.J. Brodsky, G.P. Lepage, in *Perturbative QCD*, edited by A.H. Mueller (World Scientific, Singapore, 1989).
26. M. Vanderhaeghen, P. Guichon, M. Guidal, Phys. Rev. D **60**, 094017 (1999).
27. G.P. Lepage, S.J. Brodsky, Phys. Lett. B **87**, 359 (1979); A.V. Efremov, A.V. Radyushkin, Phys. Lett. B **94**, 245 (1980).
28. M. Diehl *et al.*, Phys. Rev. Lett. **81**, 1782 (1998); M. Diehl *et al.*, arXiv:hep-ph/9901233; M.V. Polyakov, Nucl. Phys. B **555**, 231 (1999); B. Lehmann-Dronke *et al.*, Phys. Lett. B **475**, 147 (2000); Phys. Rev. D **63**, 114001 (2001); P. Hagler *et al.*, Phys. Lett. B **535**, 117 (2002); **540**, 324 (2002) (E); Eur. Phys. J. C **26**, 261 (2002).
29. I.V. Anikin, B. Pire, O.V. Teryaev, Phys. Rev. D **62**, 071501 (2000).
30. A.V. Belitsky, D. Müller, Phys. Lett. B **507**, 173 (2001).
31. E.R. Berger *et al.*, Eur. Phys. J. C **23**, 675 (2002).
32. M. Guidal, M. Vanderhaeghen, Phys. Rev. Lett. **90**, 012001 (2003); A.V. Belitsky, D. Muller, Phys. Rev. Lett. **90**, 022001 (2003).
33. B.L.G. Bakker, L.A. Kondratyuk, M.V. Terent'ev, Nucl. Phys. B **158**, 497 (1979).
34. P.L. Chung, F. Coester, B.D. Keister, W.N. Polyzou, Phys. Rev. C **37**, 2000 (1988).